Electrochemical and Microscopic Characterization of Two *meso*-Substituted A_3B and A_4 Porphyrins

BOGDAN OVIDIU TARANU[1], IULIANA SEBARCHIEVICI[1], IOAN TARANU[1], MIHAELA BIRDEANU[1], EUGENIA FAGADAR COSMA[2]*

[1]National Institute of Research-Development for Electrochemistry and Condensed Matter Timisoara, 144 Dr. A. P. Podeanu 300569, Timisoara, Romania

[2]Institute of Chemistry Timisoara of Romanian Academy, 24 M. Viteazul Av., 300223, Timisoara, Romania

Two meso-substituted porphyrins, 5-(4-pyridyl)-10,15,20-tris(phenoxy-phenyl)porphyrin and 5,10,15,20-tetra(allyloxy-phenyl)porphyrin were investigated using electrochemical and physico-chemical techniques. Cyclic voltammetry experiments outlined the comparative behaviour of the two heterocycles on the platinum, glassy carbon and fluorine-tin-oxide glass electrodes. The aggregates formed by these porphyrins were investigated using SEM, TEM and AFM microscopy. The final purpose of these studies was to extend information about the behavior of the porphyrin organization in thin layers in order to find novel applications as sensors or corrosion inhibitors.

Keywords: meso-substituted porphyrins, cyclic voltammetry, microscopy techniques

Nowadays porphyrin compounds are a class of intensely studied macromolecules [1-6], due to their particular and versatile properties conferred by the aromatic and amphoteric nature of the macrocycle and most important by possibility to tailor the peripheral substituents grafted in the *meso*- and *beta*- positions [7]. Any modifications made at the level of the porphyrin macrocycle will inevitably lead to changes in its electron density which in turn will cause the properties of the compounds to change as well [8]. This ability turns the macromolecules into suitable candidates for a wide range of applications in catalysis, photovoltaics, environmental monitoring and protection (sensors and corrosion inhibition) and non-invasive medical treatments (PDT) [9-16]. However, in order to understand the behavior of the porphyrin compounds on the road from synthesis to application, they must be studied using various analytical methods.

The present paper employs comparative cyclic voltammetry investigations on various electrode materials together with SEM, TEM and AFM advanced microscopy techniques with the purpose of gathering electrochemical, self-assembly and surface analysis data about two porphyrin structures, namely: 5-(4-pyridyl)-10,15,20-tris(phenoxy-phenyl)porphyrin (PYPPP) and 5,10,15,20-tetra(allyloxy-phenyl)porphyrin (TAPPP). Our previous experience regarding synthesis and electrochemical characterization of the porphyrin derivatives [16-20] together with these newly obtained results regarding films surface morphology will be used in the process of identifying suitable applications in sensing and corrosion inhibition.

Experimental part

The synthesis of the two porphyrin structures (PYPPP and TAPP) was performed and reported in our previous papers [19,20]. The products were obtained in fair yields. All the reagents were analytical-grade. Benzonitrile was purchased from Merck, tetrahydrofuran (THF) and tetrabutylammonium perchlorate (TBAP) were provided by Sigma-Aldrich.

Electrochemical experiments

Cyclic voltammetry was performed with a PGZ 301 Dynamic-EIS Voltammetry potentiostat equipped with VoltaMaster 4 software, using a three-electrode electrochemical glass cell. The reference was the Ag/AgCl/KCl saturated electrode and the auxiliary electrode was a platinum plate (S = 0.8 cm^2). The working electrodes were: platinum plate (S = 0.45 cm^2), glassy carbon (GC) (S = 0.28 cm^2) and fluorine doped tin oxide glass (FTO) (S = 0.28 cm^2). All potentials were referenced to the Hydrogen Standard Electrode (HSE). The electrolyte solution was benzonitrile with 0.05 mM TBAP as supporting electrolyte.

Microscopy studies

GC pallets were modified with the two porphyrins from THF solutions (0.1 mM) using the drop-casting method. Total volumes of 20 mL were deposited in steps on the surface of the GC substrates. The solution was applied on the pallets without any surface restrictions and also after entrapping the pallets in a Teflon body, thus limiting their surface (to 0.28cm^2) and preventing the spread of the porphyrins. The modified surfaces were investigated by SEM microscopy using a Field Emission - SEM/EDAX Inspect S and by AFM microscopy with a Nanosurf® EasyScan 2 Advanced Research AFM. The two porphyrins solubilized in THF (0.1 mM PYPPP and 0.04 mM TAPP) were deposited on TEM copper grids covered with carbon film and analyzed using a Titan G2 80-200 TEM/STEM microscope set at 80 KV acceleration voltage.

Results and discussions

Investigations using cyclic voltammetry

A qualitative study concerning the electrochemical behavior of the porphyrins on different electrode substrates (Pt, GC, FTO) was performed in benzonitrile solution containing 0.05M TBAP as supporting electrolyte in the presence of increasing concentrations of PYPPP(0.1, 0.2 and 0.3 mM) and TAPP porphyrins. Electrochemical studies focusing on the oxidation of PYPPP are sown in figure 1.

Curves *a* from figure 1 are the baselines recorded for the three working electrodes. In the presence of PYPPP an

* *email: efagadar@yahoo.com; Tel.: (+40) 256491818*

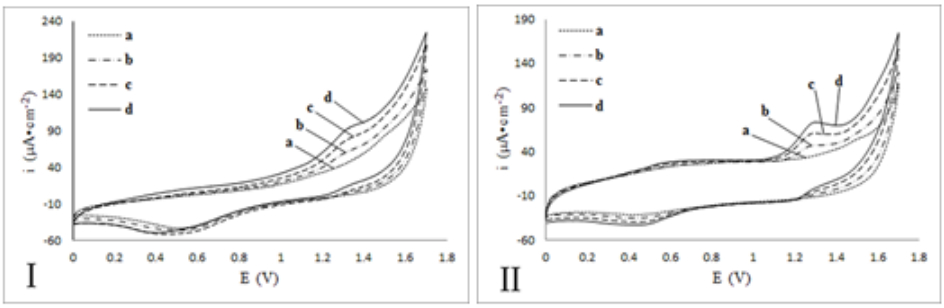

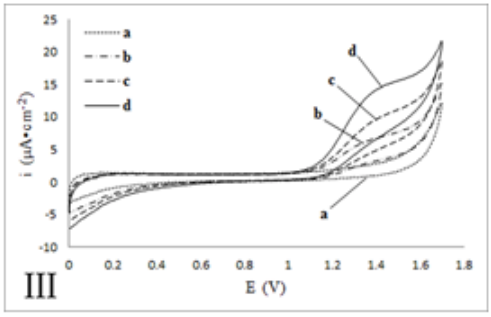

Fig. 1. Cyclic voltammograms recorded on the Pt (I), GC (II) and FTO (III) electrodes in benzonitrile solution with 0.05M TBAP, without porphyrin (*a*) and with: 0.1 mM (*b*); 0.2 mM (*c*) and 0.3 mM (*d*) PYPPP. Potential range 0 ÷ 1.7 V, cycle 3, $v = 0.1$ V•s^{-1}

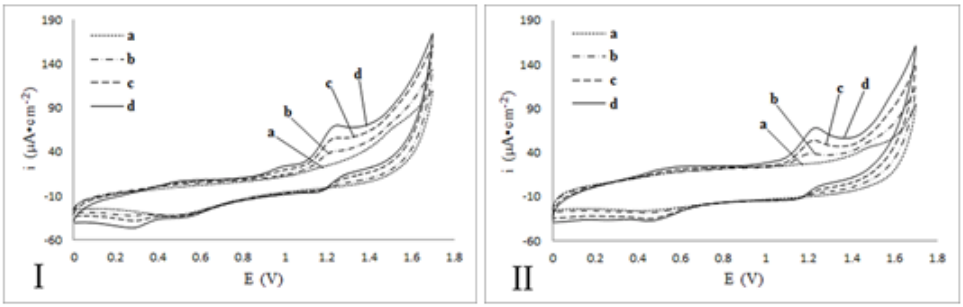

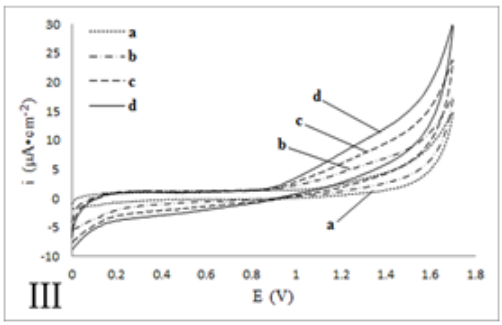

Fig. 2. Cyclic voltammograms recorded on the Pt (I), GC (II) and FTO (III) electrodes in benzonitrile solution with 0.05M TBAP, without porphyrin (*a*) and with: 0.1 mM (*b*); 0.2 mM (*c*) and 0.3 mM (*d*) TAPP. Potential range 0 ÷ 1.7V, cycle 3, $v = 0.1$ V•s^{-1}

WE	Parameters	Anodic peak dependant on PYPPP concentration			Anodic peak dependant on TAPP concentration		
		0.1 mM	0.2 mM	0.3 mM	0.1 mM	0.2 mM	0.3 mM
Pt	i [μA/cm^2]	58.3	77.11	93.72	40.10	55.33	70.24
	ε_p [V]	1.298	1.316	1.330	1.220	1.232	1.244
	ε_0 [V]	1.004	1.009	1.011	1.028	1.026	1.030
GC	i [μA/cm^2]	46.61	60.41	72.99	38.94	53.90	68.0
	ε_p [V]	1.274	1.284	1.294	1.199	1.219	1.235
	ε_0 [V]	0.997	1.015	1.013	0.944	0.948	0.953

Table 1
ELECTROCHEMICAL PARAMETERS RECORDED FOR THE Pt AND GC WORKING ELECTRODES (WE) IN THE PRESENCE OF DIFFERENT CONCENTRATIONS (0.1, 0.2 AND 0.3 mM) OF PYPPP AND TAPPP PORPHYRINS

additional anodic peak at ~ 1.3 V can be observed on the Pt and GC electrodes (curves *b, c, d* from figure 1.I and 1.II,). Its intensity increases proportionally with the porphyrin concentration (table 1). The cathodic peak observed on the baseline suffers slight changes in the presence of PYPPP. On the FTO electrode an anodic wave appears at ~ 1.4 V and its intensity is also proportional with the PYPPP concentration (fig. 1.III, curves b, c, d). For the three electrodes, the potential values of the anodic peak/wave due to PYPPP oxidation are very close to each other.

Studies concerning the electrochemical oxidation of TAPP are shown in figure 2.

Cyclic voltammograms recorded in the presence of TAPP porphyrin on the Pt and GC electrodes (fig. II.1 and II.2) show an anodic peak at ~1.2V, increasing proportionally with the porphyrin concentration. On the Pt electrode an anodic wave (~1V) and a cathodic peak (~0.3V) can also be observed. It seems that TAPP oxidation on the Pt electrode takes place in two stages, by forming firstly the cation radical and finally the dicationic form of the TAPP $^{2+}$ porphyrin.

For the FTO electrode (fig. 2.III) a large anodic wave (possibly composed of two waves very close together) at $\varepsilon_0 = 0.85$ V can be observed and its intensity increases with the TAPP concentration.

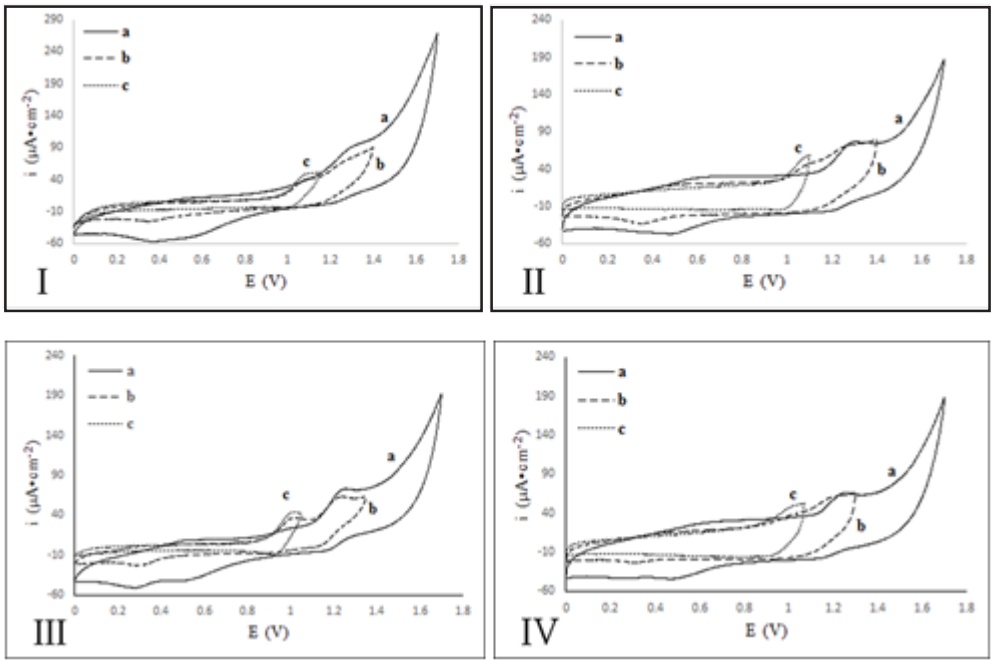

Fig. 3. Cyclic voltammograms recorded on the Pt and GC electrodes in benzonitrile solution with 0.05M TBAP in the presence of 0.3 mM PYPPP (I and II) and respectively TAPP (III and IV), at different potential ranges. Cycle 3, v = 0.1 V•s^{-1}

Table 1 shows the current densities (i), peak potentials (ε_p) and zero current potentials (ε_0) for the anodic peaks recorded in the presence of PYPPP at ~1.3V (fig. 1) and TAPP at ~1.2V (fig. 2).

The cyclic voltammograms obtained for PYPPP and TAPP on the Pt and GC electrodes at different potential ranges are shown in figure 3. The anodic processes taking place on the electrode were isolated by decreasing the polarization range. This allowed the isolation of a reversible couple (at ~1V) and a cvasi-ireversible one (at ~1.2 V) on Pt and two seemingly irreversible couples on GC. These observations indicate that porpyrin ring oxidation takes place in two stages involving cation radical and dication species for both PYPPP and TAPP.

These dicationic forms were put into evidence in case of PYPPP by UV-vis spectra, after the electrochemical experiments (fig. 4). The protonation of the inner nitrogen atoms of the porphyrin ring is produced and demonstrated by the splitting of the Soret band, into two bands, one located almost similar with that of porphyrin monomer and the second broadened and bathochromically shifted from 420 nm (pH=5.5) to 454 nm. Only one Q band is evidenced, which is the QI band that shows significant bathocromic (from 649 to 684 nm) and also hyperchromic effects [8,16,19]. The reducing of Q bands to only one is the proof for dicationic form generation and of gaining of more symmetry of the molecule.

The morphological characteristics of GC pallets modified with PYPPP and TAPP were analyzed using SEM and AFM techniques. Figure 5 shows images recorded for the PYPPP sample in 2 areas: the *centre* (5a and 5c) and *near the edge* (5b and 5d), while table 2 shows the calculated AFM parameters.

The SEM image recorded in the *centre* showed that the porphyrin behaved in two different ways: it formed a few localized grain-like aggregates, as well as ramifying branches. The SEM image obtained *near the edge* of the sample shows porphyrin deposits, including accumulations of large aggregates in the shape of uneven multilayer lamellar architectures.

The AFM image recorded in the *centre* of the sample (fig. 5c) shows only a few grain-like structures accompanied by associated ones with linear fibrous shape. *Near the edge* of the modified GC pallet (fig. 5d) large deposits (width in the range of 1,000 ÷ 5,000 nm) with

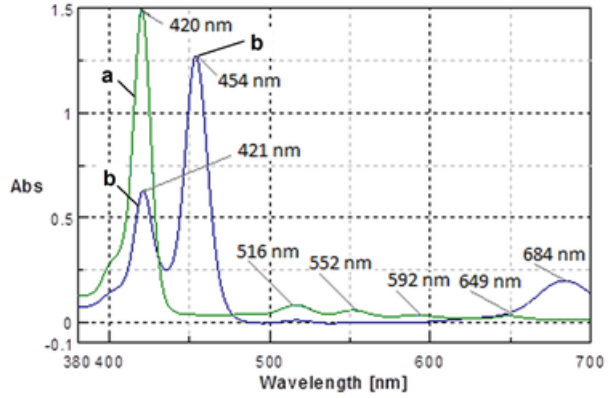

Fig. 4. Overlapped spectra of bare PYPPP porphyrin (line a) and its protonated dicationic form (line b) *SEM and AFM analyses on porphyrin modified GC substrates*

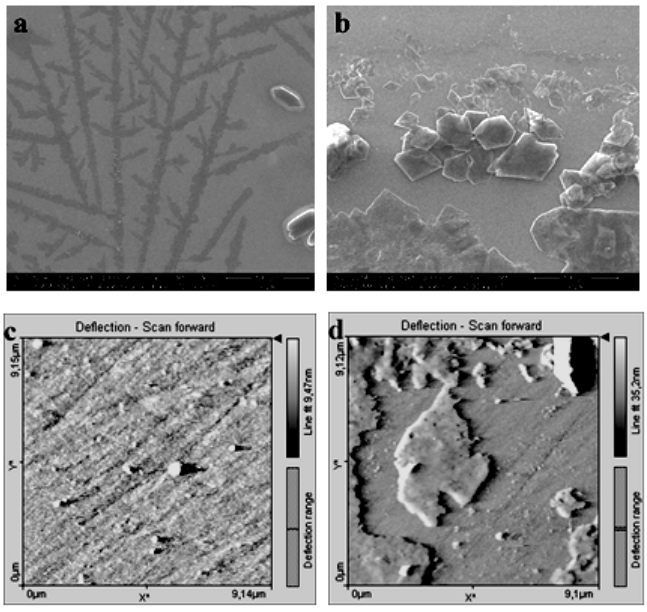

Fig. 5. SEM (a, b) and AFM micrographs (c, d) recorded in the centre (a, c) and near the edge (b, d) of the PYPPP modified GC substrate

different irregular fractal-like shapes can be observed, similar with those from SEM analysis. The values from table 2 support the observations made based on these images.

Images recorded on a TAPP modified sample, using

Table 2

PARAMETERS CALCULATED FROM AFM ANALYSIS OF PYPPP MODIFIED GC SAMPLE, IN THE CENTRE AND NEAR EDGE: SCANNED AREA (S); AVERAGE ROUGHNESS (Sa); MEAN SQUARE ROOT ROUGHNESS (Sq); MAXIMUM PEAK TO VALLEY HEIGHT (Sy); MAXIMUM PEAK HEIGHT (Sp); MAXIMUM VALLEY DEPTH (Sv); MEAN ROUGHNESS VALUE (Sm)

Sample		S (pm^2)	Sa (nm)	Sq (nm)	Sy (nm)	Sp (nm)	Sv (nm)	Sm (pm)
Unmodified GC pallet		21.14	2.6	3.2	24	11	-13	0.31
PYPPP modified GC pallet	centre	84.28	1.6	2.3	54	44	-10	27
	near edge	83.66	13	24	300	220	-72	26

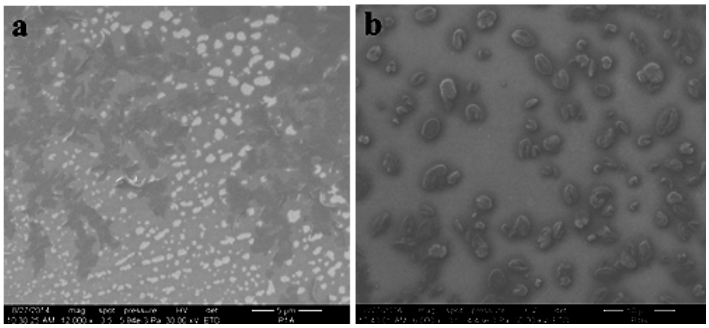

Fig. 6. SEM micrographs recorded on GC pallets in Teflon body modified with PYPPP (a) and TAPP (b)

the same methods, were previously published [18] and are referred in here only for comparison reasons. The TAPP modified GC pallet evidenced a similar behavior, being less covered in the middle and with multiple structures near the edge. SEM images showed elongated aggregates with discontinuities and cracks near the edge and ramifying branch-like deposits in the centre. AFM analysis revealed worm-like and leaf-like associations of porphyrin particles near the edge of the sample.

In order to limit the spread of the porphyrins toward the edge of the GC pallets a Teflon body was used to enclose the substrates and decrease their surface area. SEM images recorded on the PYPPP and TAPP modified substrates are shown in figure 6.

When the surface of the pallets was decreased, the porphyrins behaved differently than previously described. In case of PYPPP (fig. 6a) most aggregates look like irregular ovoidal spots linearly or circularly oriented with a few arc needle-like structures, while TAPP (fig. 6b) forms polygonal aggregates of different dimensions with cracks on their surfaces.

TEM/STEM analysis of porphyrin samples

TEM and STEM images recorded for the two porphyrins are shown in figure 7.

Images recorded on the PYPPP sample reveal circles with diameters between 70 nm and 1.85 μm (fig. 7a) and a few spherical aggregates that can be joined together, with diameters measured in the 92÷122 nm range (fig. 7b). Similar structures with molecules aligning with their macrocycles nearly parallel to the substrate surface were reported in the literature [21]. The circles or oval shapes were demonstrated to have a superior organization by aligning themselves as planetary orbits. In case of the TAPP sample the images show a few tubular crystalline aggregates (fig. 7d) having both the diameter and the length in the micrometer range, but the prominent aggregates are in the shape of rhombohedral and hexagonal plates with cracks on the surface (fig. 7c). For both porphyrins similar structures were observed in the SEM images from figure 6. All these self-assembling architectures are the result of face to face H-type aggregations and side to side J-type aggregation in which

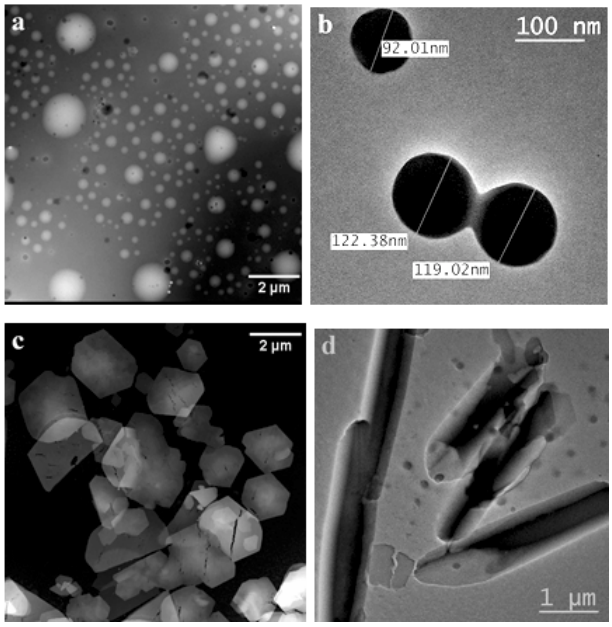

Fig. 7. Images recorded for the PYPPP (a,b) and TAPP (c,d) sample in STEM (a,c) and TEM (b,d) bright field mode

porphyrins, function of their structure and the polarity of used solvent play an important role in spiral organization producing finally microtubes of TAPP [19].

Conclusions

Electrochemical studies show that the two porphyrins suffer oxidation processes on the Pt, GC and FTO electrodes. Those processes take place in two steps, involving in the first step the formation of a π-cation radical and in the second the dication of the porphyrins [22]. The PYPPP anodic peak has a higher intensity than the TAPP peak (table 1), indicating that PYPPP is more reactive than TAPP on the Pt and GC electrodes. Also, the peak potentials are very close for the two porphyrins proving that the oxidation process takes place at the porphyrin ring and not at the level of the *meso*-substituents.

SEM and AFM analysis showed significant differences between the centre and the edge of the porphyrin modified GC samples. In all cases the centre was covered with thin layers of porphyrins, while accumulations of large aggregates were observed near the edges. When the porphyrins were deposited on restricted GC surfaces placed in a Teflon body, different aggregates were observed with a more uniform distribution. These SEM images revealed similarities with TEM/STEM data. In both cases PYPPP samples showed mostly irregular ovoidal spots with linear or circular orientation, while TAPP samples revealed polygons with cracked surfaces and tubular structures. All these self-assembling architectures are the result of face to face H-type aggregations and side to side J-type aggregation in which porphyrins function of their *meso*-substituents play an important role in spiral organization.

Taking into consideration the evidenced reactivity of the two porphyrins on the working electrodes further

approaches will focus on electrochemically modifying the surface of these substrates in order to design and develop novel potentiometric sensors.

Acknowledgements: The authors from INCEMC kindly acknowledge Programme PN contract No. 09-34 02 07 and the author Eugenia Fagadar-Cosma kindly acknowledges Institute of Chemistry Timisoara of Romanian Academy, Programme 3-Porphyrins/2015 and STAR Programme, SAFEAIR Project 76/2013.

References

1. POPA, I., FAGADAR-COSMA, G., TARANU, B.O., BIRDEANU, A. V., TARANU, I., VLASCICI, D., BIRDEANU, M., FAGADAR-COSMA, E., Dig. J. Nanomater. Bios., **9**, no. 3, 2014, p.1277
2. SUN, M., ZHANG, H., Hu, X., Liu, B., Liu, Y., Chin. J. Chem., **32**, no. 8, 2014, p.771
3. MENG, S., Xu, Z., Ge, H., ZHAO, L., ZHAO, Z, GUO, J., JI, H., LIU, T., Eur. J. Med. Chem., **92**, 2015, p.35
4. KOORIYADEN, F.R., SUJATHA, S., VARGHESE, B., ARUNKUMAR, C., J. Fluorine Chem., **170**, 2015, p.10
5. JAGADEESWARI, S., PARAMAGURU, G., RENGANATHAN, R., J. Photochem. Photobiol. A, **276**, 2014, p.104
6. IORDACHE, S., CRISTESCU, R., POPESCU, A.C., POPESCU, C.E., DORCIOMAN, G., MIHAILESCU, I.N., CIUCU, A.A., BALAN, A., STAMATIN, I., FAGADAR-COSMA, E., CHRISEY, D.B., Appl. Surf. Sci., **278**, 2013, p.207
7. VLASCICI, D., FAGADAR-COSMA, E., POPA, I., CHIRIAC, V., GIL-AGUSTI, M., Sensors, **12**, no. 6, 2012, p.8193
8. FAGADAR-COSMA, E., VLASCICI, D., BIRDEANU, M., FAGADAR-COSMA, G., Arabian J. Chem., 2014, http://dx.doi.org/10.1016/j.arabjc.2014.10.011 - on line
9. CREANGA, I., PALADE, A., LASCU, A., BIRDEANU, M., FAGADAR-COSMA, G., FAGADAR-COSMA, E., Dig. J. Nanomater. Bios., **10**, no. 1, 2015, p.315
10. BRAVO, P., ISAACS, F., RAMIREZ, G, AZOCAR, I., TROLLUND, E., AGUIRRE, M.J., J. Coord. Chem., **60**, no. 22, 2007, p.2499
11. FAGADAR-COSMA, G., TARANU, B.O., BIRDEANU, M., POPESCU, M., FAGADAR-COSMA, E., Dig. J. Nanomater. Bios., **9**, no. 2, 2014, p.551
12. YELLA, A., MAI, C-L., ZAKEERUDDIN, M.S., CHANG, S-N., HSIEH, C-H., YEH, C-Y., GRATZEL, M., Angew. Chem. Int. Ed., **53**, no. 11, 2014, p.2973
13. FAGADAR-COSMA, E., VLASCICI, D., FAGADAR-COSMA, G., PALADE, A., LASCU, A., CREANGA, I, BIRDEANU, M., CRISTESCU, R., CERNICA, I., Molecules, **19**, no. 12, 2014, p.21239
14. MARUYAMA, J., BAIER, C., WOLFSCHMIDT, H., BELE, P., STIMMING, U., Electrochim. Acta, **63**, 2012, p.16
15. ESTEVES, C.H.A., IGLESIAS, B.A., LI, R.W.C., OGAWA, T., ARAKI, K., GRUBER, J., Sens. Actuators B, **193**, 2014, p.136
16. FAGADAR-COSMA, E., CSEH, L., BADEA, V., FAGADAR-COSMA, G., VLASCICI, D., Comb. Chem. High Throughput Screening, **10**, 2007, p.466
17. TARANU, B.O., FAGADAR-COSMA, E., POPA, I. PLESU, N., TARANU, I., Dig. J. Nanomater. Bios., **9**, no. 2, 2014, p.667
18. TARANU, B.O., FAGADAR-COSMA, E., POPA, I., BIRDEANU, M, FAGADAR-COSMA, G., SFIRLOAGA, P., CREANGA, I., PALADE, A., TARANU, I., Proceedings of the 20th International Symposium on Analytical and Environmental Problems, Ed: Galbacs, Z., Szeged, Hungary, 2014, p.166-169
19. FAGADAR-COSMA, E., FAGADAR-COSMA, G., VASILE, M., ENACHE, C., Curr. Org. Chem., **16**, no. 24, 2012, p.931
20. DUDAS, Z., ENACHE, C., FAGADAR-COSMA, G., ARMEANU, I., FAGADAR-COSMA, E., Mater. Res. Bull., **45**, 2010, p.1150
21. DJURIC, T., ULES, T., GUSENLEITNER, S., KAYUNKID, N., PLANK, H., HLAWACEK, G., TEICHERT, C., BRINKMANN, M., RAMSEY, M., RESELA, R., Phys. Chem. Chem. Phys., **14**, 2012, p.262.
22. GIRAUDEAU, A., SCHAMING, D., HAO, J., FARHA, R., GOLDMANN, M., RUHLMANN, L., J. Electroanal. Chem., **638**, no. 1, 2010, p.70.

Manuscript received: 8.07.2015